Computational approaches identify novel transcription factor combinations that promote corticospinal axon growth after injury

Ishwariya Venkatesh[1*], Vatsal Mehra[1], Zimei Wang[1], Matthew T. Simpson[1], Erik Eastwood[1], Advaita Chakraborty[1], Zac Beine[1], Derek Gross[1], Michael Cabahug[1], Greta Olson[1] and Murray G. Blackmore[1*].
* These two authors contributed equally.

Author affiliations: 1 - Department of Biomedical Sciences, Marquette University, Milwaukee, WI.

Corresponding Authors - Ishwariya Venkatesh and Murray.G.Blackmore.
Department of Biomedical Sciences, Marquette University, Milwaukee, WI, 53201, USA. Phone: Email Address: ishwariya.venkatesh@marquette.edu; murray.blackmore@marquette.edu

Conflict of Interest: None

Acknowledgments: This work was supported by grants from NINDS (5R01NS083983, R21NS106309), The Craig Neilsen Foundation, The Bryon Riesch Paralysis Foundation, and computational allocations from NSF-XSEDE. We wish to thank Erik Van Newenhizen for technical assistance. The authors acknowledge ENCODE consortia for generating the developmental time-series NGS datasets used in this study. The authors declare no competing financial interests.

Abstract:
Transcription factors (TFs) act as powerful levers to regulate neural physiology and can be targeted to improve cellular responses to injury or disease. Because TFs often depend on cooperative activity, a major challenge is to identify and deploy optimal sets. Here we developed a novel bioinformatics pipeline, centered on TF co-occupancy of regulatory DNA, and used it to predict factors that improve axon growth in corticospinal tract (CST) axons when combined with a known pro-regenerative TF, Klf6. Assays of neurite outgrowth confirmed cooperative activity by 12 candidates, and *in vivo* testing showed strong promotion of CST growth upon combined expression of Klf6 and Nr5a2. Transcriptional profiling of CST neurons identified Klf6/Nr5a2-responsive gene networks involved in macromolecule biosynthesis and DNA repair. These data identify novel TF combinations that promote enhanced CST growth, clarify the transcriptional correlates, and provide a bioinformatics roadmap to detect TF synergy.

Introduction:
As they mature, neurons in the central nervous system (CNS) decline in their capacity for robust axon growth, which broadly limits recovery from injury [1–4]. Axon growth depends on the transcription of large networks of regeneration-associated genes (RAGs), and coaxing activation of these networks in adult CNS neurons is a major unmet goal [2,5]. During periods of developmental axon growth, RAG expression is supported by pro-growth transcription factors (TFs) that bind to relevant promoter and enhancer regions to activate transcription [3,6]. One factor that limits RAG expression in mature neurons is the developmental downregulation of these pro-growth TFs [2,5]. Thus identifying TFs that act developmentally to enable axon growth and supplying them to mature neurons is a promising approach to improve regenerative outcomes in the injured nervous system.

An ongoing challenge, however, is to decode the optimal set of factors for axon growth. To date, progress has centered on identifying individual TFs whose ectopic expression in mature neurons leads to improved axon growth. For example, we showed previously that the TF Klf6 is developmentally downregulated and that viral re-expression drives improved axon growth in mature corticospinal neurons, which are critical mediators of fine movement [7]. The restoration of axon growth from this and other single-factor studies remains partial, however, indicating the need for additional intervention.[7–12]. One likely possibility is that because multiple TFs generally act in a coordinated manner to regulate transcription, a more complete restoration of axon growth will depend on multiple TFs. Consistent with this, regeneration competent neurons recruit groups of interacting TFs in the hours to days post-injury, which results in transcriptional remodeling leading to reactivation of growth gene networks and functional recovery [13–15]. The need for multi-TF interventions in CNS neurons is recognized conceptually [5,16], but a major challenge has been to develop a systematic pipeline aimed at discovering growth-relevant TF combinations.

Here we developed a novel bioinformatics framework to detect cooperative TF promotion of axon growth. The framework centers on the concept of TF co-occupancy, in which functional interactions between TFs are detected by virtue of shared binding to common sets of regulatory DNA. We deployed the pipeline to predict novel TFs that potentially synergize with Klf6 to drive enhanced axon outgrowth. *In vitro* phenotypic screening confirmed cooperative TF activity for 12 candidates, and two independent bioinformatic analyses converged to prioritize interest in a core of three factors, Nr5a2, Rarb, and Eomes. Systematic tests of forced TF

co-expression *in vivo* using a pyramidotomy model of axon injury revealed strong and consistent promotion of corticospinal tract axon growth by combined expression of Klf6 and Nr5a2. Finally, transcriptional profiling of purified CST neurons revealed transcriptional correlates to the evoked growth, notably genes modules related to biosynthesis and DNA repair. Overall we have identified novel combinations of transcription factors that drive enhanced axon growth in mature CNS neurons, and provide a generalized computational roadmap for the discovery of cooperative activity between TFs with potential application to a wide range of neural activities.

Results:

In vitro screening identifies TFs that synergize with Klf6 to drive increased neurite outgrowth:

TFs that functionally synergize often do so by binding DNA in close proximity and initiating complementary transcriptional mechanisms [17–20]. Thus, analysis of TF co-occupancy can reveal novel instances of cooperation between TFs[21,22]. It was shown previously that the TF Klf6 is expressed in CST neurons during developmental periods of axon growth, is down-regulated during postnatal maturation, and that forced re-expression in adult neurons modestly enhances axon growth[7]. We therefore reasoned that during development, additional TFs likely co-occupy regulatory elements alongside Klf6 and cooperate to regulate transcription. We further hypothesized that identifying these co-occupiers and supplying them to adult neurons along with Klf6 may lead to further enhancement of axon growth after injury.

To identify potential Klf6 co-occupiers, we first assembled a list of genes that decline in expression as cortical neurons mature, using data from corticospinal motor neurons (CSMNs) *in vivo* and cortical neurons ages *in vitro*[2324] **(Fig.1A)**. Genes common to both datasets were selected for further analysis. To tighten the focus on genes that contribute to axon growth, we selected those genes associated with Gene Ontology terms linked to axon growth, including cytoskeleton organization, microtubule-based transport, nervous system development, and regulation of growth. **Supplementary Table 1** summarizes the final list of 308 developmentally downregulated pro-growth genes and their associated GO terms. For each gene, promoters were assigned as 1500 bp upstream/300 bp downstream of the transcription start site (TSS). To assign enhancers we took advantage of recent advances in machine learning-based algorithms, deploying the activity-by-contact (ABC) pipeline to reconstruct functional enhancer-gene pairs during active periods of developmental axon growth[25]. Utilizing open-access ENCODE datasets of chromatin accessibility, H3K27Ac enrichment, HiC, and expression datasets from embryonic forebrain, ABC identified a total of 1230 enhancers linked to the selected growth-relevant genes[26]. Each gene was associated with between 1 and 13 enhancers (Mean 6 +/- 3 SEM), 80% of which were located 10-1500 kb from the transcription start site. The full list of enhancer-gene pairs with genomic coordinates is summarized in **Supplementary Table 1**. Finally, to predict the binding of Klf6 and potential co-occupying TFs, we examined promoters and enhancers using an anchored TF motif analysis algorithm. This algorithm scans sequences for the canonical Klf6 binding motif and then identifies TF binding motifs that are over-represented in nearby DNA[27]. The result was 62 candidate TFs that were predicted to frequently co-occur with Klf6 in pro-growth promoters, pro-growth enhancers, or both.

We next used high content screening to test the prediction that these candidate TFs functionally synergize with Klf6 to enhance neurite outgrowth. Using a well-established screening platform, postnatal cortical neurons received candidate genes by plasmid electroporation and were cultured at low density on laminin substrates, followed two days later by automated tracing to quantify neurite outgrowth.[1,7,12,24,28–30]. As expected, forced

expression of Klf6 alone increased neurite outgrowth by 28% (+/- 4.37% SEM) compared to EBFP control. To establish the assay's sensitivity to combined treatments we confirmed that co-expression of Klf6 with a known synergizer, Stat3[7], further elevated lengths to 61% (+/- 5.59%), significantly above the level of Klf6 alone (p-value<.01, ANOVA with post-hoc Fisher's LSD). Notably, of the 62 candidate TFs, twelve significantly elevated neurite length above the level of Klf6 alone ("hard hits") (p-value <0.05, ANOVA with post-hoc Fisher's LSD), and an additional five missed statistical significance but improved growth in two of three replicate experiments ("soft hits") **(Fig.1B;** see **Supplementary Table S2** for detailed screening data**)**. Interestingly, all twelve hit TFs came from the one-third of candidates that were predicted to co-occupy with Klf6 in both promoters and enhancers, and no hits came from TFs predicted to co-occupy solely in promoters or in enhancers **(Fig.1C)**. These data support the ability of co-occupancy analysis to predict functional interactions between TFs and emphasize the importance of scanning both promoter and enhancer elements.

We then used network analyses to prioritize interest in the twelve "hard hit" TFs. First, using open-access TF binding data, top transcriptional targets of the twelve hit TFs were used to generate individual TF-target gene networks. These networks were then merged, expanded to bring in immediately connected genes based on known interactions, and restructured to move genes with maximal connections to the center and minimal connections to the periphery. This resulted in a unified network with a core of TFs predicted to exert maximal influence, surrounded by shells of TFs with progressively lower connectivity (**Fig. 1C**). Notably, during the expansion step, Klf6 itself was among the genes that were spontaneously added to the network. Klf6 was the only added TF to be placed in the core, even as additional pro-growth TFs including Sox11, Stat3, Myc, and Jun appeared in inner shells. The appearance of these TFs and their central positions in the network substantiates the premise that the constructed network is Klf6-centered and relevant to axon growth[2,7–11,31–33]. Moreover, all five of the "soft hit" TFs also appeared but were placed in outer shells of the network, hinting at interactions near the threshold of screening sensitivity. Most importantly, three hit TFs (Nr5a2, Eomes, Rarb) occupied the core with Klf6, prioritizing subsequent interest. Thus an integrated pipeline of co-occupancy analyses, high content screening, and network analyses point toward three TFs as potentially cooperative with Klf6.

For independent validation, we performed a second analysis, this time starting from a previously published set of genes that are upregulated in cortical neurons *in vitro* upon forced expression of Klf6[7]. We again performed a network analysis of Klf6-upregulated genes, constructing functionally related subnetworks, and then examined gene promoters within each subnetwork for the enrichment of TF motifs. This independent analysis detected enrichment for the motifs of seven factors, which remarkably included the 3 "core" TFs identified above **(Fig.1D)**. Thus, genes that respond to Klf6 over-expression are enriched for the recognition motifs of Eomes, Nr5a2, and Rarb, supporting the hypothesis that they cooperate with Klf6 to activate pro-growth gene networks.

Nr5a2 synergizes with Klf6 and Rarb to drive enhanced CST sprouting following pyramidotomy injury:

We next asked whether forced expression of the three hit TFs, singly or in conjunction with Klf6, can promote the growth of CST axons *in vivo*. TFs and tdTomato tracer were delivered to adult mice by cortical injection of AAV, with AAV-Cre acting as control and also included in single-gene treatments to equalize the viral load in all animals **(See Supplementary Table 3)**. Mice received unilateral pyramidotomy, followed eight weeks later by quantification of cross-midline sprouting of corticospinal (CST) axons in the cervical spinal cord, measured at 200, 400, and 600μm from the midline **(Fig.2A)**. Injuries were confirmed by unilateral ablation of PKCγ in

spinal sections, and axon counts were normalized to tdTomato+ axons in the medullary pyramids. Raw images of all animals are provided in **Supplementary Figs 1-3**. In addition to Cre, we also included Nkx3.2, a non-hit/non-core TF, as an additional negative control; RNAscope or immunohistochemistry confirmed overexpression of all TFs **(Supplementary. Fig. 4)**. As expected, Klf6 expression significantly increased normalized axon counts at all distances across the midline ($p<.01$, 2-way ANOVA) **(Fig.2G,N)**. When expressed singly, none of the candidate TFs significantly elevated axon growth above the level of control **(Fig.2D-F, J-K, N)**. When combined with Klf6, however, significant effects emerged **(Fig.2D-N)**. Most notably, co-expression of Nr5a2 with Klf6 consistently elevated axon counts above that of Klf6 alone, and above the maximum growth in Cre controls in all animals. Co-expression of Rarb with Klf6 drove growth that exceeded Klf6 alone at 200μm from the midline **(Fig.2N)**. In three of nine animals, combined Eomes/Klf6 expression yielded high axon counts, but this effect was inconsistent and did not reach statistical significance **(Fig.2N)**. Finally, as, expected, Nkx3.2 produced no significant elevation in axon growth above the level of Klf6 alone **(Fig.2H, N)**. In summary, these data identify robust synergy between Klf6 and candidate TFs, most notably Nr5a2.

We then performed a second *in vivo* pyramidotomy experiment to confirm Nr5a2's synergy with Klf6, and to determine whether Nr5a2 might similarly potentiate the growth of other pro-growth TFs. AAV delivery, injury, and axon quantification were identical to the first experiment, and detailed histology is available in **Supplementary Figs 1-3)**. In this experiment, Nr5a2 acted as the base gene, to which control, Klf6, or Rarb were added. Consistent with the prior experiment, combined Nr5a2/Klf6 expression elevated CST growth above the level of either alone **(Fig.3E)**. Moreover, axon growth in the lowest Klf6/Nr5a2 animal still exceeded that in the maximum control animal, illustrating the strength and consistency of the effect. Interestingly, combined Nr5a2 and Rarb also elevated CST growth above the level of either alone **(Fig.3A-E)**. This effect did not appear as striking as that of Nr5a2/Klf6, but nevertheless substantiates the ability of network analysis to predict functional TF cooperation. Thus combinations of TFs, rationally selected based on the basis of predicted co-occupancy of pro-growth regulatory DNA, can enhance CST axon growth *in vivo*.

Combined Klf6-Nr5a2 treatment leads to the upregulation of gene modules related to macromolecule biosynthesis and DNA repair:

To probe the underlying mechanisms of growth promotion, we profiled the transcriptional consequences of single and combined expression of Klf6 and Nr5a2 in CST neurons. To isolate CST neurons, nuclear-localized fluorophores and TFs were expressed by cervical injection of Retro-AAV2, which results in highly efficient and selective transgene expression by retrograde transduction[34] **(Fig.4A-B)**. Animals received pyramidotomy injury, followed one week later by purification of labeled nuclei of CST neurons by flow cytometry, isolation of messenger RNA, and construction and sequencing of RNA libraries. Differential gene expression was determined using EdgeR software. Compared to tdTomato control, single expression of Klf6 resulted in the upregulation of 209 transcripts (transcripts with FPKM>5 and log2fold change>1; p-value < 0.05, FDR < 0.05). Reminiscent of prior findings in cultured neurons[7], network analysis of Klf6-responsive genes revealed subnetworks with functions highly relevant to axon growth, including CNS development, neuron projection development, migration, adhesion, and cytoskeleton organization **(Fig.4C-D)**. Indeed, neuron projection and cytoskeleton networks comprised more than 60% of Klf6-responsive genes, consistent with the effects of Klf6 overexpression on axon growth **(Fig.4E-F)**. Single overexpression of Nr5a2 had little unique effects on gene expression, with only 27 transcripts identified as upregulated only in the Nr5a2 group, and 131

transcripts shared with the Klf6 treatment group. Dual Klf6/Nr5a2 expression, however, drove upregulation of 192 transcripts that were not significantly increased by either alone **(Supplementary Table 4).** Interestingly, network analysis of these transcripts revealed modules involved in macromolecule biosynthesis, DNA repair, and development, all of which showed substantial increases in the net expression above control levels **(Fig.4G-J)**. Intriguingly, recent analyses of regeneration-competent peripheral neurons also showed that genes involved in macromolecule biosynthesis and DNA repair are upregulated in the course of successful regeneration[14], supporting their potential involvement in axon growth. In aggregate, these data substantiate the ability of forced Klf6 expression to activate gene networks relevant to axon growth and point toward the ability of dual Klf6/Nr5a2 expression to activate gene networks involved in macromolecule synthesis and DNA repair as a likely explanation for their combined enhancement of axon growth.

Discussion

Using interlocking bioinformatics approaches, high content screening, and *in vivo* testing, we have identified new TF combinations that synergize to enhance CST axon growth. In addition, transcriptional profiling and network analyses provide molecular correlates to the evoked responses. These findings clarify cellular functions that drive axon extension and serve as a roadmap for ongoing efforts to discover novel combinatorial gene treatments to promote regenerative axon growth.

Klf6 belongs to the KLF family of transcription factors, which have well-studied roles in regulating axon growth[1,7,12,35]. Retinoic acid receptor Beta (Rarb) and Nuclear Receptor Subfamily 5, Group A, Member 2 (Nr5a2/LRH-1) both belong to the nuclear receptor family of transcription factors, with diverse functions in development and cellular metabolism[36]. Rarb has previously been linked to axon growth, and a Rarb agonist is under evaluation for clinical efficacy in a brachial plexus avulsion model of injury[37]. In contrast, Nr5a2 is unstudied in the context of axon extension. It has, however, been linked to the differentiation of neural stem cells and to cellular reprogramming, and can replace Oct4 in the reprogramming of murine somatic cells to pluripotent cells[38,39]. Our present work adds to the growing body of evidence that TFs involved in neuronal differentiation may positively influence axon growth[9,13].

An important finding is that although Nr5a2 does not improve axon growth when expressed individually, it strongly potentiates the effect of overexpressed Klf6. The importance of combinatorial gene activity for axon growth, as opposed to single factor effects, is increasingly recognized [2,5,40]. Regeneration-competent cell types such as zebrafish retinal ganglion cells and peripherally injured sensory neurons respond to axotomy by upregulating groups of TFs that likely synergize to drive regenerative axon growth [14,15,41]. An unmet challenge, however, has been to turn the conceptual appreciation for the role of TF synergy into an operational pipeline to discover effective gene combinations for axon extension in the injured nervous system. Whereas prior efforts have focused on direct protein-protein interactions to predict TF synergy[41], here we exploited the concept of TF co-occupancy. A search for factors with recognition motifs in proximity to those of Klf6 yielded a set of 62 candidate TFs, which was further narrowed by phenotypic screening. A key observation from the cell culture experiments is that none of the hit TFs were predicted to co-occupy solely in promoter regions; rather, all hit TFs were characterized by predicted co-occupancy in both promoters and enhancers. This suggests a key role for enhancer elements in regulating pro-growth gene transcription, in line with the recent finding in DRG neurons that modulation of enhancers may be critical for transcriptional activation of growth genes[13,42]. Finally, guided by network analysis of the screening results, a

systematic campaign of combinatorial testing *in vivo* identified highly consistent enhancement of CST axon growth by combined expression of Klf6 and Nr5a2. To our knowledge, this is the first evidence of TF synergy in driving growth of axons following CNS injury *in vivo.* Although these experiments were anchored on Klf6, these data show a pipeline that can be re-deployed to identify additional TF combinations that synergize to drive growth, or potentially other cellular functions.

A key insight from the current work is to clarify *in vivo,* in purified CST neurons, the transcriptional events that are triggered by Klf6, Nr5a2, and the two together. Forced expression of Klf6 activates highly interconnected groups of genes with functions in various aspects of axon growth spanning terms such as Neuron Projection Development, Cytoskeleton organization, Motility, and Adhesion. This finding illustrates the potential of TF-based interventions to trigger broad changes in gene expression; it is most likely that improvements in axon growth reflect the net change in a wide set of transcripts, as opposed to acting through any single target. Combined Klf6/Nr5a2 expression, which led to large and consistent increases in axon growth above those triggered by Klf6 alone, also caused the upregulation of unique modules of genes with functions in macromolecule biosynthesis and DNA repair. These modules were activated by neither Klf6 nor Nr5a2 alone, suggesting that enhanced biosynthesis and/or DNA repair contribute to the enhanced growth in Klf6/Nr5a2-treated animals. A role for the biosynthesis of macromolecules is highly plausible, as active growth depends on new cellular material. Indeed, regeneration-competent zebrafish RGCs and mammalian DRGs also respond to injury by upregulating genes involved in macromolecule biosynthesis[15,13,14]. Moreover, a very recent study in DRG neurons found that peripheral injury, which triggers axon growth, resulted in a sustained upregulation of genes involved in biosynthesis. In contrast, a central injury that does not trigger regeneration led to eventual downregulation, suggesting that a reduction in biosynthesis pathways may restrict axon growth after spinal injury[43]. Our new findings regarding the effects of Klf6/Nr5a2 add to multiple lines of evidence that the upregulation of genes involved in biosynthesis may be an evolutionarily conserved molecular signature of neurons mounting a successful growth response.

Regarding DNA repair pathways, it is interesting to note that increased cellular metabolism and transcription frequently lead to DNA damage[44,45]. Moreover, disruption of DNA repair machinery in mouse retinal progenitors or cortical progenitors leads to reduced, disturbed trajectories of axon growth and guidance[46,47]. Thus during development, proper axon growth may require efficient DNA repair machinery. Similarly, peripherally injured DRG neurons upregulate several DNA damage response marker genes, and blocking this response leads to reduced neurite outgrowth *in vitro* and impaired regeneration *in vivo*[48]. The finding that combined Klf6/Nr5a2 expression activates genes involved in DNA repair suggests the intriguing hypothesis that this repair machinery may aid successful axon regrowth in CNS neurons; future work can address this notion.
In summary, a new bioinformatic and screening platform, centered on the concept of TF co-occupancy, has revealed synergy between transcription factors Klf6 and Nr5a2 that leads to improved axon growth after CNS injury.

Methods:

Identification of developmentally downregulated, growth-relevant transcripts:

All expression datasets used to identify developmentally down-regulated genes are deposited at NCBI GEO (In vivo CSMNs data by[23] - GSE2039; In vitro primary neurons aged in culture by[24], SRP151916). *In vitro*

RNA-Seq datasets were processed as described previously [24] . Trimmed reads were mapped to the rat reference genome [UCSC, Rat genome assembly: Rnor_6.0] using HISAT2 aligner software (unspliced mode along with–qc filter argument to remove low quality reads prior to transcript assembly)[49]. Transcript assembly was performed using Stringtie [50] and assessed through visualization on UCSC Genome Browser. Differential gene expression analysis was performed using Ballgown software (Default parameters) [50]. Transcripts were considered significant if they met the statistical requirement of having a corrected p-value of <0.05, FDR <0.05.

For the *in vivo* CSMN microarray datasets, weighted correlation network analysis (WGCNA) was performed as described previously [51]. First, relevant microarray datasets (GSE2039) were loaded into R and basic pre-processing of data was performed to remove outlier data and handle probes with missed data. Outlier data was identified by performing hierarchical clustering to detect array outliers. Numbers of missing samples in each probe profile were counted and probes with extensive numbers of missing samples were removed. All pre-processing steps were performed as described in [51]. Next, a weighted correlation network was constructed by creating a pairwise pearson correlation matrix, which was transformed into an adjacency matrix using a power of 10. Then, topological overlap was calculated to measure network interconnectedness and average linkage hierarchical clustering was done to group genes on the basis of the topological overlap dissimilarity measure. Finally, using a dynamic tree-cutting algorithm we identified 20 gene modules. Gene modules with developmental down-regelation in expression of 2-fold and above were isolated for ontology analyses. Gene ontology analyses were performed using Database for Annotation, Visualization and Integrated Discovery (DAVID) Bioinformatics Resource[52] and genes with terms relevant to axon growth (FDR<0.05) based on literature review were user-selected for further analyses.

Enhancer Identification

Enhancers relevant to pro-growth genes were identified by running the Activity-by-contact (ABC) algorithm[25] using code described here - https://github.com/broadinstitute/ABC-Enhancer-Gene-Prediction. ENCODE datasets used for the analysis are - ATAC-Seq (ENCSR310MLB, ENCSR836PUC), H3K27Ac histone ChIP-seq (ENCSR094TTT, ENCSR428OEK), RNA-seq (ENCSR362AIZ, ENCSR080EVZ) and HiC (GSE96107). The algorithm has three sequential steps – definition of candidate enhancers, quantification of enhancer activity and calculation of ABC scores. For definition of candidate enhancers, indexed and sorted bam files of ATAC-Seq and H3K27Ac ChIP-seq datasets were supplied and peaks were called using MACS2, with the argument --nStrongestPeaks 15000. For quantification of enhancer activity, reads counts were calculated using peak files processed in the previous step to yield a final list of candidate enhancer regions with ATAC-seq and H3K27ac ChIP-seq read counts within gene bodies and promoters. Finally, ABC scores were calculated using arguments --hic_resolution 5000, -scale_hic_using_powerlaw and a threshold of 0.02. The default threshold of 0.02 corresponds to approximately 70% recall and 60% precision. All enhancer-gene pairs that passed the above threshold were used for subsequent analyses.

Co-occupancy motif analyses

Transcription factor binding site/motif analysis on pro-growth gene promoters and enhancers was performed using opossum v3.0 software[27]. For promoter analyses, the list of pro-growth genes was supplied along with promoter co-ordinates to be used for scanning (upstream/downstream of TSS – 1000/300 bps). For enhancer motif analyses, a unified file containing a list of FASTA formatted sequences corresponding to pro-growth enhancer regions was supplied.

Mouse anchored TF- cluster analyses were performed using search parameters – JASPAR CORE profiles that scan all vertebrate profiles with a minimum specificity of 8 bits, conservation cut-off of 0.40, matrix score threshold of 90%, and results sorted by Z-score >=10. TFs were sorted into three categories – TFs with over-represented sites within pro-growth promoters, TFs with over-represented sites within pro-growth enhancers and TFs with over-represented binding sites within both pro-growth promoters and enhancers.

Network analyses

Hit TF-target gene networks were constructed using ENCODE ChIP-Seq data for hit TFs using the Harmonizome database[53]. For each of the 12 hit TFs, TF target gene lists were retrieved from Harmonizome individually and merged before visualization on the Cytoscape platform (v3.7.1). Cytoscape plug-ins ClueGO and CluePedia were used for network visualization. iRegulon plug-in on the Cytoscape platform was used to expand the network one-level and bring in additional regulators. Next, we calculated connectivity scores to assign centrality using the Network Analyzer option within Cytoscape 3.7.1. TFs were ranked in descending order of connectivity scores to assign centrality. Core TFs were those TFs that had the highest connectivity scores and were centrally located in the network, followed by TFs with decreasing connectivity scores that occupied peripheral positions in the network. Upstream regulator analysis on Klf6 target genes was run on differentially expressed genes listed in[7] using motif analyses described above. Motif analyses were done in batches such that each batch had genes belonging to one functional sub-network to identify Klf6 synergizers by functional category.

Cloning and virus production:

Constructs for candidate genes were purchased from Dharmacon or Origene, and relevant accession numbers for all 62 candidate TFs are summarized in Supplementary Table 2. H2B-mNeongreen sequence was codon-optimized and synthesized by Genscript, based on the amino acid sequence of [54]. For viral production, genes were cloned into an AAV-CAG backbone (Addgene-Plasmid #59462) using standard PCR amplification, as described in [12]. Maxipreps were prepared by Qiagen Endo-free kits and fully sequenced, and AAV2-Retro was produced at the University of North Carolina Viral Vector Core and brought to $1x10^{13}$ particles per ml in sterile saline prior to injection. Viruses were mixed at a 3:3:2 ratio of combinatorial test genes and tracer; viral treatments are detailed in **Supplementary Table 3**.

Cortical cell culture and analysis of neurite outgrowth

All animal procedures were approved by the Marquette University Institutional Animal Care and Use Committee. Cortical neurons were prepared from early postnatal (P5-P7) Sprague Dawley rat pups (Harlan), with each experimental replicate derived from a separate litter. Procedures for dissociation, transfection, immunohistochemistry, imaging, and neurite outgrowth analysis were performed as in[7]. For all cell culture experiments, neurite length from a minimum of 200 cells per treatment was averaged, and each experiment was repeated a minimum of three times on separate days. These averaged values were the basis for ANOVA with Fisher's multiple comparisons. Neurite outgrowth values, number of cells analyzed for every screening experiment are summarized in Supplementary Table 2.

Viral delivery to cortical neurons and pyramidotomy injuries

In vivo experiments were performed in a double-blind fashion, with non-involved lab personnel maintaining

blinding keys. Animals were randomized prior to viral treatment, with each surgical day, including equal numbers from each group. Cortical neurons were transduced using intracerebral microinjection as described in[7,8]. Mice were anesthetized with ketamine/xylazine (100/10 mg/kg, IP), mounted in a stereotactic frame, and skull exposed and scraped away with a scalpel blade. 0.5 µl of virus particles were delivered at two sites located 0 and 0.5 mm anterior, −1.3 mm lateral from Bregma and at a depth of 0.55 mm, at a rate of 0.05 ul/min using a pulled glass micropipette connected to a 10 µl Hamilton syringe driven by a programmable pump (Stoelting QSI). After each injection, the needle was left in place for 1 minute to minimize viral solution flow upwards. Unilateral pyramidotomy was performed as described in[8,12]. Briefly, a ventral midline incision was made to expose the occipital bone, the ventrocaudal part of which was removed using fine rongeurs. The dura was punctured, and the right pyramid cut completely using a micro feather scalpel.

RNAScope

RNAscope kits are commercially available from Advanced Cell Diagnostics (ACD). We utilized the Multiplex v2 system for all RNAScope experiments (Cat-323100,ACD). Mouse brains were snap-frozen on dry ice and cryosectioned (25µm). Slides were baked at 60°C for 40 mins followed by RNAScope procedures according to manufacturer's instructions. Briefly, hydrogen peroxide solution was applied to baked slices and incubated for 10 mins at RT. Next, slices were incubated in boiling antigen retrieval solution (<98 °C) for 5 mins. Following retrieval, slices were washed in Nuclease free water three times, 5 mins per wash. Then, brain slices were dehydrated in 100% ethanol briefly followed by treatment with ProteaseIII for 20 mins at 40°C. Following protease incubation, slices were washed in Nuclease free water three times, 5 mins per wash and probes were applied and allowed to incubate for 2 hours at 40°C. The following probes were purchased off the catalog- RNAscope® Probe - Mm-Klf6 (Cat- 426901, ACD), RNAscope® Probe - Mm-Nkx3-2 (Cat- 526401, ACD),RNAscope® Probe - Mm-Rarb (Cat- 463101, ACD). We designed a custom probe for Nr5a2, targeting a region common to all variants(RNAscope® Probe - Mm-Nr5a2-O1-C2, Cat- 547841-C2, ACD). All all probes were detected with TSA plus fluorophore used at 1:750 dilution. Before mounting the slices, a brief 5 minute incubation with DAPI was performed to label the nuclei. All RNAScope experiments were carried out between 1-3 days post cryosectioning to ensure tissue integrity.

Immunohistochemistry

Adult animals were perfused with 4% paraformaldehyde (PFA) in 1X-PBS (15710-Electron Microscopy Sciences, Hatfield, PA), brains, and spinal cords removed, and post-fixed overnight in 4% PFA. Transverse sections of the spinal cord were embedded in 12% gelatin in 1X-PBS (G2500-Sigma Aldrich, St.Louis, MO) and cut via Vibratome to yield 100 µm sections. Sections were incubated overnight with primary antibodies PKCγ (SC C-19, Santa Cruz, Dallas, TX, 1:500, RRID: AB_632234), rinsed and then incubated for two hours with appropriate Alexa Fluor-conjugated secondary antibodies (Thermofisher, Waltham, MA, 1:500.) Fluorescent images were acquired using Olympus IX81 or Zeiss 880LSM microscopes.

Quantification of axon growth

Axon growth was quantified from four 100 µm transverse sections of the spinal cord of each animal that spanned C2 to C6 spinal cord. Starting from a complete series of transverse sections, the rostral-most was selected from C2 as identified by the morphology of the ventral horns of the spinal cord, and the next three selected at 1.6mm intervals in the caudal direction. Each section was imaged on Nikon confocal microscope (Nikon AR1+) using a 20X Plan Apochromatic (MRD00205, NA 0,75) objective, gathering 20 µm of images at

5 µm intervals and then creating a maximum intensity projection. On the resulting image, virtual lines of 10 µm width were placed at 200, 400, and 600 µm from the midline and intersection of tdTomato+ axons with these lines were quantified. For normalization, 100 µm transverse sections of the medullary pyramids were prepared by vibratome sectioning and imaged on a Nikon confocal microscope (Nikon AR1+) using a 60X Apochromatic Oil DIC N2 (MRD71600, NA 1.4) objective. Seven virtual lines of 10 µm width were distributed evenly across the medial/lateral axis of the medullary pyramid, the number of tdTomato+ axons visible in each was determined, and the total number of axons extrapolated based on the area of the entire pyramid and the area of the sampled regions. Fiber index was calculated as the average number of axons at each distance from the midline across the 4 replicate spinal sections, divided by the calculated number of axons detected in the pyramid. Counting of digital images was performed by three blinded observers, with final values reflecting the average. Exclusion criteria for pyramidotomy experiments were animals with less than 80% decrease in PKCγ in the affected CST.

RNA-Seq data generation and analysis

Equal numbers of male and female mice were used in every experiment in concordance with NIH guidelines. Adult mice received retrograde injections of viral vectors for Ctrl treatment, Klf6 alone treatment, or combined Klf6+ Nr5a2 treatment. One week later, animals were challenged with pyramidotomy injuries, as described above. One week post-injury, animals were euthanized, and the motor cortices were dissected. Dissected cortices were minced finely using razor blades and transferred to pre-chilled 15 ml Dounce homogenizer filled with 3 ml Nuclear release buffer (320mM Sucrose, 5mM Cacl2, 3mM MgCl2, 10mM Tris-HCL, 0.3% Igepal). Tissue was dounced 15X while on ice and filtered sequentially via a 50um, 20um filter, and used as input for flow cytometry. Dissociated nuclei were flow-sorted on a BD FACS Melody using an 80um nozzle to a goal of approximately 30,000 events. Nuclei sorted into Trizol were lysed, and RNA was extracted according to manufacturer's instructions. Only samples with a RIN score of 8 and above were used for library prep. Total RNA was used for library prep using Takara SMARTer stranded total RNA-Seq kit v2 according to the manufacturer's instructions. Samples were sequenced at the University of Wisconsin-Madison Genomics core to a depth of 25 million paired-end reads on an Illumina HiSeq platform, with two replicates per treatment. Raw FASTQ files were fed into ENCODE consortia RNA-Seq pipeline described here - https://github.com/ENCODE-DCC/rna-seq-pipeline. Read alignment was performed using STAR[55] and transcript quantification performed using Kallisto[56]. Transcript counts from Kallisto were used for performing differential gene expression (DEG) analyses using EdgeR[57]. Transcripts were considered significant if they met the statistical requirement of having a corrected p-value of <0.05, FDR <0.05. Differentially expressed genes were further filtered to only include transcripts with FPKM > 5 and log2Foldchange > 1. RNA-Seq datasets have been deposited with NCBI GEO (SRP151916). Network analysis on significantly differentially expressed genes (upregulated) was performed on the cytoscape platform v3.7.1 using plug-ins clueGo and CluePedia. Functional analysis mode was selected and the following GO categories were selected for analyses- GO Biological Process, KEGG pathways, Reactome Pathways and Wiki pathways. Network specificity was set to medium and GO tree interval was set between 3-8. GO term kappa score was set to default values (0.4) and leading group term was set to rank by highest significance. Lastly, GO term fusion was also selected and only sub-networks with significantly enriched GO terms were used to generate network visualizations ($p < 0.05$, Right-sided hypergeometric test with Bonferroni correction, Cytoscape).Expression heat-maps were assembled using heatmapper.ca using average linkage and Euclidean distance parameters for clustering.

Figure legends:

Fig 1: In vitro screening and network analyses identify a novel pro-growth transcription factor network

(A) A graphical overview of the bioinformatic steps and packages used to predict TFs that co-occupy regulatory DNA associated with developmentally downregulated, growth-relevant transcripts (B) Postnatal cortical neurons were transfected with control plasmid, Klf6 with control, or Klf6 combined with 62 candidate TFs. After two days in culture, automated image analysis (Cellomics) quantified neurite lengths normalized to the average of on-plate controls. The solid black line indicates the average control length, and the shaded grey box the standard deviation around the average increase of Klf6 alone. Combined expression of Klf6 and Vp16-Stat3 showed an expected increase in neurite length above Klf6 alone, confirming assay sensitivity (yellow bar, p-value <0.0001, ANOVA with post-hoc Fishers). 12 candidate TFs significantly enhanced neurite outgrowth when combined with KLF6 (orange bars, p-value <0.05, ANOVA with post-hoc Fishers), and 5 more enhanced growth in 2 of 3 replicates but missed the cut-off for statistical significance (blue bars). (C) Hit TFs were used to build networks. All hit TFs derived from candidates with predicted Klf6-co-occupancy in both promoters and enhancers. Rarb, Eomes, and Nr5a2 were located in the network core, where Klf6 itself also appeared during network construction. Several soft hit TFs (blue) and established pro-growth TFs (pink) spontaneously populated outer shells. (D) Network analysis was performed on transcripts upregulated by Klf6 overexpression in culture neurons, followed by motif analysis of gene promoters within each module. Of the ten TF motifs with the highest enrichment, seven were hit TFs from the screening experiment (orange), including Rarb, Eomes, and Nr5a2.

Figure 2. Nr5a2 synergizes with Klf6 to promote CST sprouting. (A) Adult mice received cortical AAV delivery of single or combinatorial TFs and contralateral pyramidotomy. (B) Co-injected tdTomato labeled CST axons, visible in the cross-section of the medullary pyramids. (C) PKCϒ immunohistochemistry confirmed unilateral ablation of the CST (arrow). (D-M) Cross-midline sprouting of CST axons was quantified in transverse spinal sections. Candidate TFs administered singly did not significantly elevate axon growth, whereas Nr5a2 and Rarb elevated growth above the level of Klf6 alone. (#p=.052, * p<.05, **p<.01, 2-way ANOVA, post-hoc Dunnett's). Scale bars are 1mm. PKCy, medulla, and spinal images from all animals are in Supp. Figs 1-3.

Figure 3. Nr5a2 synergizes with Rarb to promote CST sprouting. (A-D) Adult mice received cortical AAV delivery of single or combinatorial TFs and contralateral pyramidotomy. Co-injected AAV-tdTomato labeled CST axons. Elevated cross-midline sprouting of CST fiber is evident in animals treated with combined Nr5a2 and Rarb (arrows, D). (E) Cross-midline sprouting of CST axons was quantified in transverse spinal sections. Nr5a2 administered alone had no significant effect on axon growth (blue bars), but increased axon growth when combined with either Klf6 or Rarb, significantly above the level of either alone (green and pink bars, respectively). (**p<.01, 2-way ANOVA, post-hoc Dunnett's). Scale bars are 1mm. PKCy, medulla, and spinal images from all animals are in Supp. Figs 1-3.

Figure 4. Combined Klf6, Nr5A2 treatment induces expression of gene modules involved in macromolecule biosynthesis and DNA repair. (A) Overview of sample collection for RNA-Seq analysis. (B) Shows nuclei before and after FANS, confirming the successful purification of mNeongreen+ nuclei. (C) Regulatory network analysis of genes upregulated after Klf6 overexpression revealed sub-networks enriched for distinct functional categories highly relevant to axon growth. Nodes correspond to target genes and edges to

multiple modes of interaction (physical, shared upstream regulators, shared signaling pathways, and inter-regulation). Only significantly enriched GO categories were included in the network analysis ($p < 0.05$, Right-sided hypergeometric test with Bonferroni correction, Cytoscape). (D) Heatmap showing the selection of differentially expressed genes between control and Klf6 treatment. (E) shows the number of genes within each functional sub-network (top) and the total fpkm values in each in control and Klf6 overexpression groups. (F) indicates the percent change in expression within each module, revealing that CNS development and migration/motility modules showed highest gain in expression upon Klf6 treatment (G) Regulatory network analysis of genes upregulated after combined Klf6 and Nr5a2 overexpression revealed sub-networks enriched for functions in macromolecule biosynthesis and DNA repair ($p < 0.05$, Right-sided hypergeometric test with Bonferroni correction, Cytoscape) (H) Heatmap showing selection of differentially expressed genes in DNA repair and macromolecule biosynthesis modules. Genes that are upregulated (green) and downregulated (red) relative to control are shown. Color values indicate average FPKM expression values as shown in the legend. Columns correspond to treatment groups and rows to genes. (I) shows the number of genes within functional sub-networks (top) and the sum of fpkm within each in control and combined Klf6/Nr5a2 treatment (bottom). (J) indicates the percent change in FPKM values within each module, revealing that combined KLF6 and Nr5a2 treatment most affect genes in DNA repair and Macromolecule biosynthesis modules.

Supplementary Figure 1. Summary of in vivo CST sprouting after single or combinatorial expression of candidate TFs. (A) illustrates the unilateral pyramidotomy injury and indicates the approximate location of images. (B) shows a transverse section of the spinal cord, eight weeks after pyramidotomy, with CST axons labeled by tdTomato. Vertical lines show the sampling regions in which axonal profiles were counted at 200, 400, and 600µm from the midline. (C,D) provide example images from all animals in two in vivo experiments; where images are missing, the reason for exclusion is indicated.

Supplementary Figure 2. Summary of tdTomato label in CST axons in the medulla, used to normalize CST counts in the spinal cord. (A) illustrates the unilateral pyramidotomy injury and indicates the approximate location of images. (B) shows a transverse section of an example medullary pyramid, nine weeks after cortical injection with AAV-TF treatment and AAV-tdTomato tracer, in which CST axons appear as red (tdTomato+) puncta as they intersect the plane of the section. The pyramid is outlined, and vertical boxes indicate the regions in which axons were counted. Total axon numbers were estimated by multiplying axon counts by the total sampling area, divided by the total medullary area. (C,D) provide example images from all animals in two in vivo experiments; where images are missing, the reason for exclusion is indicated.

Supplementary Figure 3. Summary of PKCy signal in the cervical spinal cord, used to verify unilateral ablation of the CST. (A) illustrates the unilateral pyramidotomy injury and indicates the approximate location of images. (B) shows a transverse section of the cervical spinal cord, eight weeks after pyramidotomy injury, with PKCy signal (green) readily detectable in the intact but not transected CST (arrow). (C,D) provide example images of the dorsal columns after PKCγ immunohistochemistry from all animals in two in vivo experiments; where images are missing, the reason for exclusion is indicated.

Supplementary Figure 4. RNAscope and immunohistochemistry confirm the expression of candidate transcription factors. Adult mice received cortical injection of AAV expressing candidate transcription factors, followed by pyramidotomy injury. Eight weeks later animals were perfused, cryostat sections were

prepared from the cortex, and RNAscope or appropriate antibodies were used to probe for expression. (A-D) show coronal sections of the motor cortex with the injection site indicated by arrows. RNAscope signal from probes directed against the expressed TFs is present at the injection site, which at higher magnification (A'-D') shows the characteristic punctate detection of transcripts. E and E' show detection of Eomes by immunohistochemistry. (F-H) show dual detection of Klf6 and Nr5A2 transcripts in a mouse cortex injected with both AAV-Klf6 and AAV-Nr5A2, with the majority of cells expressing both transcripts. Scale bars are 500μm in A-D, and 10μm in A'-D' and F-H.

Bibliography

1. Moore, D. L. *et al.* KLF family members regulate intrinsic axon regeneration ability. *Science* **326**, 298–301 (2009).
2. Venkatesh, I. & Blackmore, M. G. Selecting optimal combinations of transcription factors to promote axon regeneration: Why mechanisms matter. *Neurosci. Lett.* **652**, 64–73 (2017).
3. O'Donovan, K. J. Intrinsic Axonal Growth and the Drive for Regeneration. *Front. Neurosci.* **10**, 486 (2016).
4. He, Z. & Jin, Y. Intrinsic Control of Axon Regeneration. *Neuron* **90**, 437–451 (2016).
5. Mahar, M. & Cavalli, V. Intrinsic mechanisms of neuronal axon regeneration. *Nat. Rev. Neurosci.* **19**, 323–337 (2018).
6. Goldberg, J. L. How does an axon grow? *Genes Dev.* (2003).
7. Wang, Z. *et al.* KLF6 and STAT3 co-occupy regulatory DNA and functionally synergize to promote axon growth in CNS neurons. *Sci. Rep.* **8**, 12565 (2018).
8. Wang, Z., Reynolds, A., Kirry, A., Nienhaus, C. & Blackmore, M. G. Overexpression of Sox11 Promotes Corticospinal Tract Regeneration after Spinal Injury While Interfering with Functional Recovery. *Journal of Neuroscience* **35**, 3139–3145 (2015).
9. Norsworthy, M. W. *et al.* Sox11 Expression Promotes Regeneration of Some Retinal Ganglion Cell Types but Kills Others. *Neuron* **94**, 1112–1120.e4 (2017).
10. Luo, X. *et al.* Enhanced Transcriptional Activity and Mitochondrial Localization of STAT3 Co-induce Axon Regrowth in the Adult Central Nervous System. *Cell Rep.* **15**, 398–410 (2016).
11. Belin, S. *et al.* Injury-Induced Decline of Intrinsic Regenerative Ability Revealed by Quantitative Proteomics. *Neuron* **86**, 1000–1014 (2015).
12. Blackmore, M. G. *et al.* Kruppel-like Factor 7 engineered for transcriptional activation promotes axon regeneration in the adult corticospinal tract. *Proceedings of the National Academy of Sciences* **109**, 7517–7522 (2012).
13. Palmisano, I. *et al.* Epigenomic signatures underpin the axonal regenerative ability of dorsal root ganglia sensory neurons. *Nat. Neurosci.* **22**, 1913–1924 (2019).
14. Li, S. *et al.* The transcriptional landscape of dorsal root ganglia after sciatic nerve transection. *Sci. Rep.* **5**, 16888 (2015).
15. Dhara, S. P. *et al.* Cellular reprogramming for successful CNS axon regeneration is driven by a temporally changing cast of transcription factors. *Sci. Rep.* **9**, 14198 (2019).

16. Hilton, B. J. & Bradke, F. Can injured adult CNS axons regenerate by recapitulating development? *Development* **144**, 3417–3429 (2017).
17. Kidder, B. L., Yang, J. & Palmer, S. Stat3 and c-Myc genome-wide promoter occupancy in embryonic stem cells. *PLoS One* **3**, (2008).
18. He, A., Kong, S. W., Ma, Q. & Pu, W. T. Co-occupancy by multiple cardiac transcription factors identifies transcriptional enhancers active in heart. *Proceedings of the National Academy of Sciences* **108**, 5632–5637 (2011).
19. Liu, L. *et al.* Modeling co-occupancy of transcription factors using chromatin features. *Nucleic Acids Res.* **44**, e49–e49 (2015).
20. Lee, Y. & Zhou, Q. Co-regulation in embryonic stem cells via context-dependent binding of transcription factors. *Bioinformatics* **29**, 2162–2168 (2013).
21. Wang, J. *et al.* Factorbook.org: a Wiki-based database for transcription factor-binding data generated by the ENCODE consortium. *Nucleic Acids Res.* **41**, D171–D176 (2013).
22. Wang, J. *et al.* Sequence features and chromatin structure around the genomic regions bound by 119 human transcription factors. *Genome Res.* **22**, 1798–1812 (2012).
23. Arlotta, P. *et al.* Neuronal Subtype-Specific Genes that Control Corticospinal Motor Neuron Development In Vivo. *Neuron* **45**, 207–221 (2005).
24. Venkatesh, I., Mehra, V., Wang, Z., Califf, B. & Blackmore, M. G. Developmental Chromatin Restriction of Pro-Growth Gene Networks Acts as an Epigenetic Barrier to Axon Regeneration in Cortical Neurons. *Dev. Neurobiol.* **78**, 960–977 (2018).
25. Fulco, C. P. *et al.* Activity-by-contact model of enhancer-promoter regulation from thousands of CRISPR perturbations. *Nat. Genet.* **51**, 1664–1669 (2019).
26. Gerstein, M. B. *et al.* Architecture of the human regulatory network derived from ENCODE data. *Nature* **489**, 91–100 (2012).
27. Kwon, A. T., Arenillas, D. J., Hunt, R. W. & Wasserman, W. W. oPOSSUM-3: Advanced Analysis of Regulatory Motif Over-Representation Across Genes or ChIP-Seq Datasets. *G3: Genes|Genomes|Genetics* **2**, 987–1002 (2012).
28. Callif, B. L., Maunze, B., Krueger, N. L., Simpson, M. T. & Blackmore, M. G. The application of CRISPR technology to high content screening in primary neurons. *Mol. Cell. Neurosci.* (2017) doi:10.1016/j.mcn.2017.01.003.
29. Simpson, M. T. *et al.* The tumor suppressor HHEX inhibits axon growth when prematurely expressed in developing central nervous system neurons. *Mol. Cell. Neurosci.* **68**, (2015).
30. Blackmore, M. G. *et al.* High content screening of cortical neurons identifies novel regulators of axon growth. *Mol. Cell. Neurosci.* **44**, 43–54 (2010).
31. Fagoe, N. D., Attwell, C. L., Kouwenhoven, D., Verhaagen, J. & Mason, M. R. J. Overexpression of ATF3 or the combination of ATF3, c-Jun, STAT3 and Smad1 promotes regeneration of the central axon branch of sensory neurons but without synergistic effects. *Hum. Mol. Genet.* **24**, 6788–6800 (2015).
32. Lerch, J. K., Martínez-Ondaro, Y. R., Bixby, J. L. & Lemmon, V. P. cJun promotes CNS axon growth. *Mol. Cell. Neurosci.* **59**, 97–105 (2014).
33. Mehta, S. T., Luo, X., Park, K. K., Bixby, J. L. & Lemmon, V. P. Hyperactivated Stat3 boosts axon regeneration in the CNS. *Exp. Neurol.* **280**, 115–120 (2016).
34. Wang, Z., Maunze, B., Wang, Y., Tsoulfas, P. & Blackmore, M. G. Global Connectivity and Function of Descending Spinal Input Revealed by 3D Microscopy and Retrograde Transduction. *J. Neurosci.* **38**,

10566–10581 (2018).
35. Wang, Z., Winsor, K., Nienhaus, C., Hess, E. & Blackmore, M. G. Combined chondroitinase and KLF7 expression reduce net retraction of sensory and CST axons from sites of spinal injury. *Neurobiol. Dis.* **99**, 24–35 (2017).
36. Robinson-Rechavi, M., Escriva Garcia, H. & Laudet, V. The nuclear receptor superfamily. *J. Cell Sci.* **116**, 585–586 (2003).
37. Yip, P. K. *et al.* Lentiviral vector expressing retinoic acid receptor β2 promotes recovery of function after corticospinal tract injury in the adult rat spinal cord. *Hum. Mol. Genet.* **15**, 3107–3118 (2006).
38. Hale, M. A. *et al.* The nuclear hormone receptor family member NR5A2 controls aspects of multipotent progenitor cell formation and acinar differentiation during pancreatic organogenesis. *Development* **141**, 3123–3133 (2014).
39. Stergiopoulos, A. & Politis, P. K. Nuclear receptor NR5A2 controls neural stem cell fate decisions during development. *Nat. Commun.* **7**, 12230 (2016).
40. Liu, Y. *et al.* A Sensitized IGF1 Treatment Restores Corticospinal Axon-Dependent Functions. *Neuron* **95**, 817–833.e4 (2017).
41. Chandran, V. *et al.* A Systems-Level Analysis of the Peripheral Nerve Intrinsic Axonal Growth Program. *Neuron* **89**, 956–970 (2016).
42. Puttagunta, R. *et al.* PCAF-dependent epigenetic changes promote axonal regeneration in the central nervous system. *Nat. Commun.* **5**, 3527 (2014).
43. Ewan, E. E., Carlin, D., Goncalves, T. M., Zhao, G. & Cavalli, V. Ascending dorsal column sensory neurons respond to spinal cord injury and downregulate genes related to lipid metabolism. doi:10.1101/2020.05.07.083584.
44. Haffner, M. C., De Marzo, A. M., Meeker, A. K., Nelson, W. G. & Yegnasubramanian, S. Transcription-induced DNA double strand breaks: both oncogenic force and potential therapeutic target? *Clin. Cancer Res.* **17**, 3858–3864 (2011).
45. Sebastian, R. & Oberdoerffer, P. Transcription-associated events affecting genomic integrity. *Philos. Trans. R. Soc. Lond. B Biol. Sci.* **372**, (2017).
46. Onishi, K. *et al.* Genome Stability by DNA Polymerase β in Neural Progenitors Contributes to Neuronal Differentiation in Cortical Development. *J. Neurosci.* **37**, 8444–8458 (2017).
47. Baleriola, J. *et al.* Increased neuronal death and disturbed axonal growth in the Polμ-deficient mouse embryonic retina. *Sci. Rep.* **6**, 25928 (2016).
48. Krishnan, A. *et al.* A BRCA1-Dependent DNA Damage Response in the Regenerating Adult Peripheral Nerve Milieu. *Mol. Neurobiol.* **55**, 4051–4067 (2018).
49. Kim, D., Langmead, B. & Salzberg, S. L. HISAT: a fast spliced aligner with low memory requirements. *Nat. Methods* **12**, 357–360 (2015).
50. Pertea, M., Kim, D., Pertea, G. M., Leek, J. T. & Salzberg, S. L. Transcript-level expression analysis of RNA-seq experiments with HISAT, StringTie and Ballgown. *Nat. Protoc.* **11**, 1650–1667 (2016).
51. Langfelder, P. & Horvath, S. WGCNA: an R package for weighted correlation network analysis. *BMC Bioinformatics* **9**, 559 (2008).
52. Huang, D. W., Sherman, B. T. & Lempicki, R. A. Systematic and integrative analysis of large gene lists using DAVID bioinformatics resources. *Nat. Protoc.* **4**, 44–57 (2009).
53. Rouillard, A. D. *et al.* The harmonizome: a collection of processed datasets gathered to serve and mine knowledge about genes and proteins. *Database* **2016**, (2016).

54. Shaner, N. C. *et al.* A bright monomeric green fluorescent protein derived from Branchiostoma lanceolatum. *Nat. Methods* **10**, 407–409 (2013).
55. Dobin, A. *et al.* STAR: ultrafast universal RNA-seq aligner. *Bioinformatics* **29**, 15–21 (2013).
56. Bray, N. L., Pimentel, H., Melsted, P. & Pachter, L. Near-optimal probabilistic RNA-seq quantification. *Nat. Biotechnol.* **34**, 525–527 (2016).
57. Robinson, M. D., McCarthy, D. J. & Smyth, G. K. edgeR: a Bioconductor package for differential expression analysis of digital gene expression data. *Bioinformatics* **26**, 139–140 (2010).

Figure 4

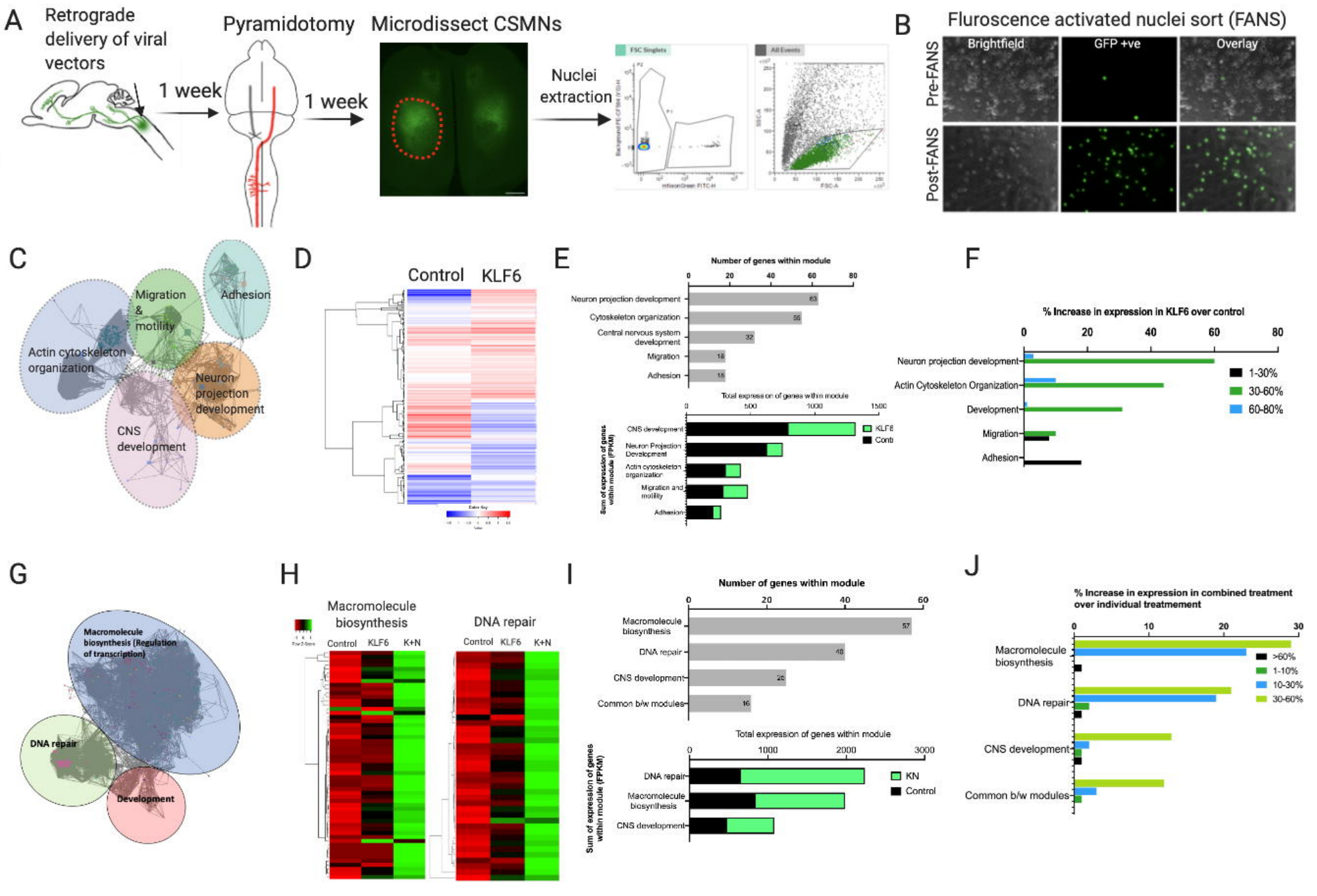
A
Retrograde delivery of viral vectors
1 week
Pyramidotomy
1 week
Microdissect CSMNs
Nuclei extraction
B
Fluroscence activated nuclei sort (FANS)
Brightfield
GFP +ve
Overlay
Pre-FANS
Post-FANS
C
Migration & motility
Adhesion
Actin cytoskeleton organization
Neuron projection development
CNS development
D
Control
KLF6
E
Number of genes within module
Neuron projection development
Cytoskeleton organization
Central nervous system development
Migration
Adhesion
Total expression of genes within module
Sum of expression of genes within module (FPKM)
CNS development
Neuron Projection Development
Actin cytoskeleton organization
Migration and motility
Adhesion
KLF6
Contr
F
% Increase in expression in KLF6 over control
Neuron projection development
Actin Cytoskeleton Organization
Development
Migration
Adhesion
1-30%
30-60%
60-80%
G
Macromolecule biosynthesis (Regulation of transcription)
DNA repair
Development
H
Macromolecule biosynthesis
DNA repair
Control
KLF6
K+N
I
Number of genes within module
Macromolecule biosynthesis
DNA repair
CNS development
Common b/w modules
Total expression of genes within module
Sum of expression of genes within module (FPKM)
DNA repair
Macromolecule biosynthesis
CNS development
KN
Control
J
% Increase in expression in combined treatment over individual treatmement
Macromolecule biosynthesis
DNA repair
CNS development
Common b/w modules
>60%
1-10%
10-30%
30-60%

Figure 3

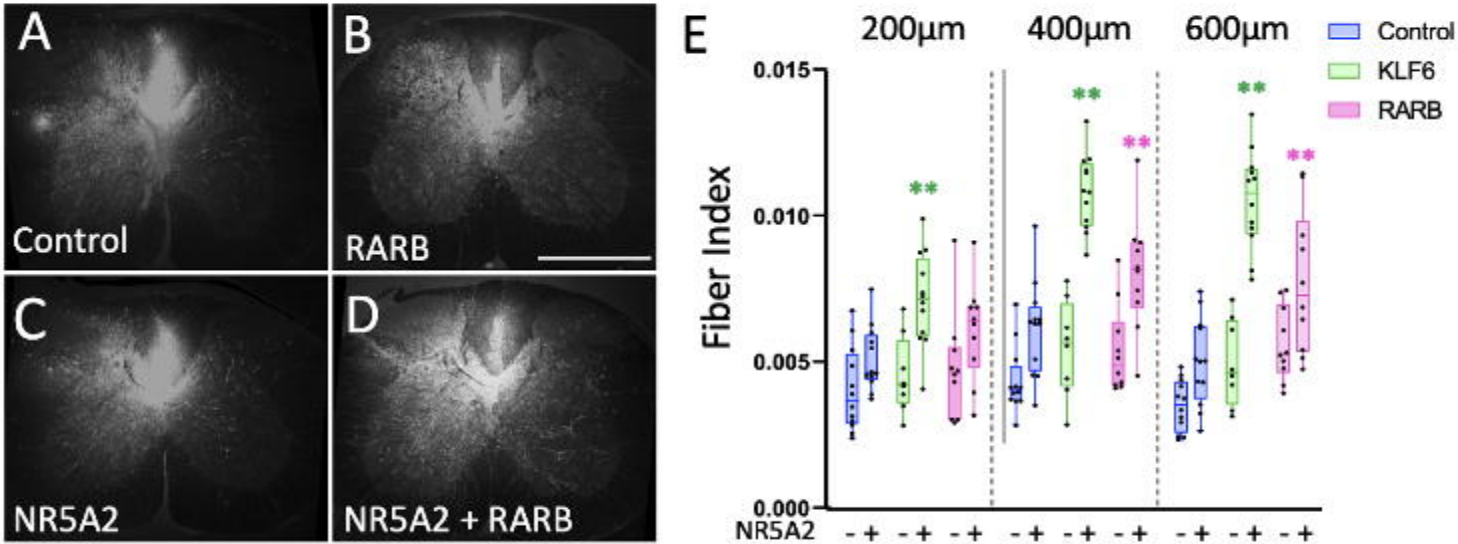
A
Control
B
RARB
C
NR5A2
D
NR5A2 + RARB
E
200µm
400µm
600µm
Control
KLF6
RARB
Fiber Index
0.015
0.010
0.005
0.000
**
NR5A2
- + - + - + - + - + - + - + - + - +

Figure 2

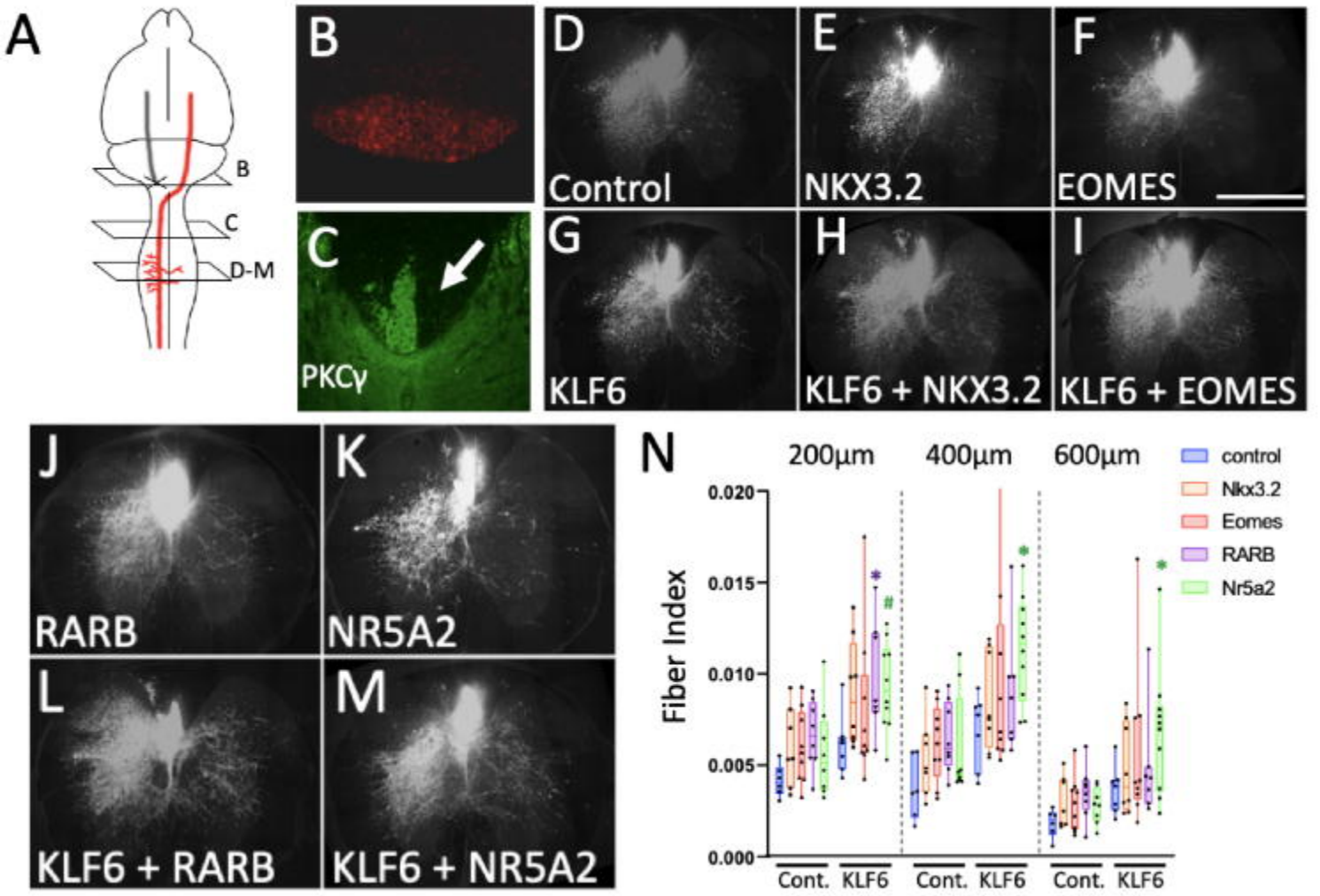
A
B
C
D-M
B
C
PKCγ
D
Control
E
NKX3.2
F
EOMES
G
KLF6
H
KLF6 + NKX3.2
I
KLF6 + EOMES
J
RARB
K
NR5A2
L
KLF6 + RARB
M
KLF6 + NR5A2
N
200µm
400µm
600µm
control
Nkx3.2
Eomes
RARB
Nr5a2
Fiber Index
0.020
0.015
0.010
0.005
0.000
Cont.
KLF6
Cont.
KLF6
Cont.
KLF6

Figure 1

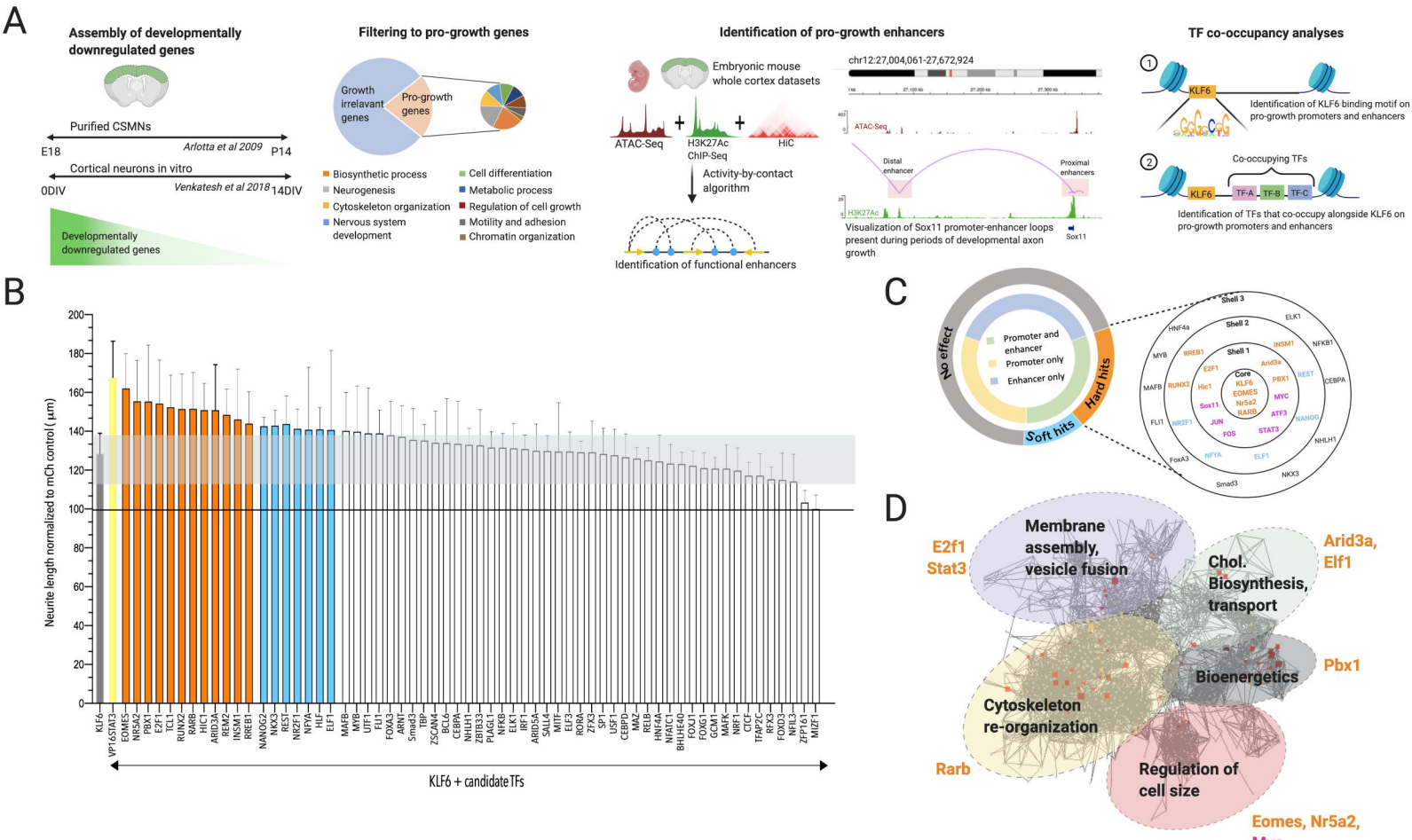
A
Assembly of developmentally downregulated genes
Purified CSMNs
E18
P14
Arlotta et al 2009
Cortical neurons in vitro
0DIV
14DIV
Venkatesh et al 2018
Developmentally downregulated genes
Filtering to pro-growth genes
Growth irrelavant genes
Pro-growth genes
Biosynthetic process
Neurogenesis
Cytoskeleton organization
Nervous system development
Cell differentiation
Metabolic process
Regulation of cell growth
Motility and adhesion
Chromatin organization
Identification of pro-growth enhancers
Embryonic mouse whole cortex datasets
ATAC-Seq
H3K27Ac ChIP-Seq
HiC
Activity-by-contact algorithm
Identification of functional enhancers
chr12:27,004,061-27,672,924
ATAC-Seq
Distal enhancer
Proximal enhancers
H3K27Ac
Sox11
Visualization of Sox11 promoter-enhancer loops present during periods of developmental axon growth
TF co-occupancy analyses
KLF6
Identification of KLF6 binding motif on pro-growth promoters and enhancers
Co-occupying TFs
TF-A
TF-B
TF-C
Identification of TFs that co-occupy alongside KLF6 on pro-growth promoters and enhancers
B
Neurite length normalized to mCh control (µm)
KLF6 + candidate TFs
C
No effect
Hard hits
Soft hits
Promoter and enhancer
Promoter only
Enhancer only
Shell 3
Shell 2
Shell 1
Core
KLF6
EOMES
Nr5a2
RARB
D
Membrane assembly, vesicle fusion
E2f1
Stat3
Chol. Biosynthesis, transport
Arid3a, Elf1
Bioenergetics
Pbx1
Cytoskeleton re-organization
Rarb
Regulation of cell size
Eomes, Nr5a2, Myc